Article

Cell Reports

ULK1 O-GlcNAcylation Is Crucial for Activating VPS34 via ATG14L during Autophagy Initiation

Graphical Abstract

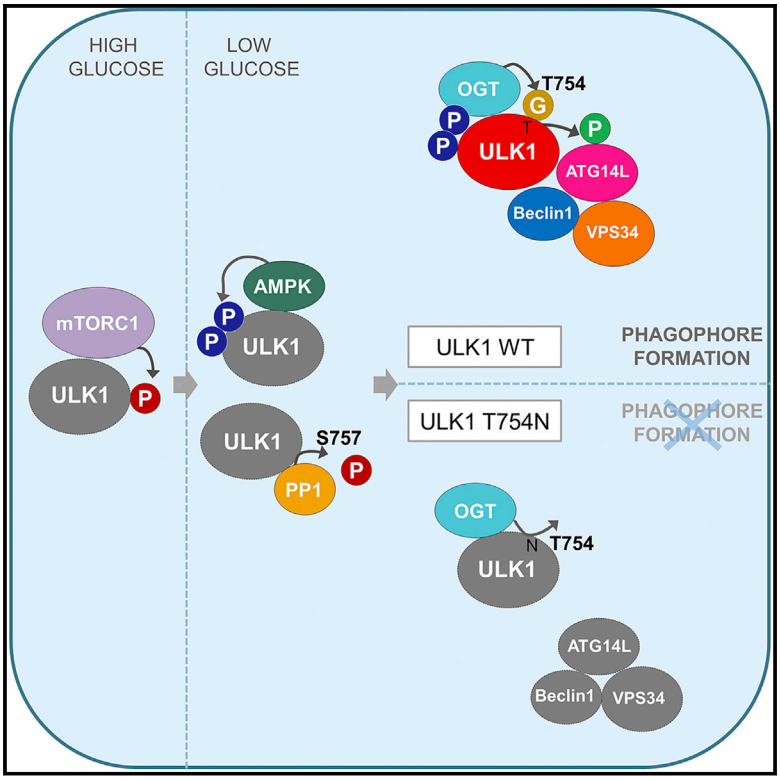

Authors

Ki Eun Pyo, Chang Rok Kim, Minkyoung Lee, Jong-Seo Kim, Keun Il Kim, Sung Hee Baek

Correspondence

kikim@sookmyung.ac.kr (K.I.K.), sbaek@snu.ac.kr (S.H.B.)

In Brief

Autophagy initiation is regulated by ULK1, a serine/threonine kinase. Pyo et al. demonstrate that ULK1 is O-GlcNAcylated on threonine 754 by OGT upon glucose starvation. O-GlcNAcylation of ULK1 is crucial for activating VPS34 via ATG14L. Our findings provide new insights into the crosstalk between dephosphorylation and O-GlcNAcylation during the autophagy process.

Highlights

- ULK1 is O-GlcNAcylated by OGT on the threonine 754 site
- ULK1 O-GlcNAcylation is positively correlated to autophagosome formation
- ULK1 O-GlcNAcylation is crucial for activating VPS34 via ATG14L
- Dephosphorylation and O-GlcNAcylation of ULK1 governs autophagy initiation

Pyo et al., 2018, Cell Reports *25*, 2878–2890
December 4, 2018
https://doi.org/10.1016/j.celrep.2018.11.042

CellPress

OPEN ACCESS
CellPress

Cell Reports
Article

ULK1 O-GlcNAcylation Is Crucial for Activating VPS34 via ATG14L during Autophagy Initiation

Ki Eun Pyo,[1] Chang Rok Kim,[1] Minkyoung Lee,[1] Jong-Seo Kim,[2] Keun Il Kim,[3,*] and Sung Hee Baek[1,4,*]
[1]Creative Research Initiatives Center for Epigenetic Code and Diseases, Department of Biological Sciences, Seoul National University, Seoul 08826, South Korea
[2]Center for RNA Research, Institute for Basic Science, Department of Biological Sciences, Seoul National University, Seoul 08826, South Korea
[3]Department of Biological Sciences, Sookmyung Women's University, Seoul 04310, South Korea
[4]Lead Contact
*Correspondence: kikim@sookmyung.ac.kr (K.I.K.), sbaek@snu.ac.kr (S.H.B.)
https://doi.org/10.1016/j.celrep.2018.11.042

SUMMARY

Unc-51-like-kinase 1 (ULK1) is a target of both the mechanistic target of rapamycin (mTOR) and AMP-activated protein kinase (AMPK), whose role is to facilitate the initiation of autophagy in response to starvation. Upon glucose starvation, dissociation of mTOR from ULK1 and phosphorylation by AMPK leads to the activation of ULK1 activity. Here, we provide evidence that ULK1 is the attachment of O-linked N-acetylglucosamine (O-GlcNAcylated) on the threonine 754 site by O-linked N-acetylglucosamine transferase (OGT) upon glucose starvation. ULK1 O-GlcNAcylation occurs after dephosphorylation of adjacent mTOR-dependent phosphorylation on the serine 757 site by protein phosphatase 1 (PP1) and phosphorylation by AMPK. ULK1 O-GlcNAcylation is crucial for binding and phosphorylation of ATG14L, allowing the activation of lipid kinase VPS34 and leading to the production of phosphatidylinositol-(3)-phosphate (PI(3)P), which is required for phagophore formation and initiation of autophagy. Our findings provide insights into the crosstalk between dephosphorylation and O-GlcNAcylation during autophagy and specify a molecular framework for potential therapeutic intervention in autophagy-related diseases.

INTRODUCTION

Autophagy refers to the catabolic process through which cells eliminate cytoplasmic components by delivering them to lysosomes (Mizushima et al., 2010). It is characterized by several steps, involving nucleation and elongation of the isolated membrane, followed by the double-membrane structure, forming a vesicle to fuse with a lysosome to yield autolysosome. Cargo is then degraded and recycled in the autolysosome (Abada and Elazar, 2014). Such metabolites generated by autophagy are reused as sources of energy or building blocks for the synthesis of new macromolecules.

Autophagy initiation is regulated by Unc-51-like kinase 1 (ULK1), which functions as a serine/threonine kinase and is mainly present in the cytosolic organelles such as endoplasmic reticulum (ER), lysosomes, mitochondria, and cytosol. The formation of the ULK1, ATG13, and FIP200 complex is not altered by nutrient conditions nor mechanistic target of rapamycin (mTOR) signaling in mammals (Hosokawa et al., 2009; Shang and Wang, 2011). When activated, ULK1 phosphorylates ATG13 and FIP200, triggering complex activity in the initial steps of autophagosome biogenesis (Jung et al., 2009).

There are two major upstream regulators of ULK1: the mTOR complex 1 (mTORC1) and AMP-activated protein kinase (AMPK). mTORC1 is a protein complex consisting of mTOR serine/threonine kinase, Raptor, MLST8, PRAS40, and DEP domain-containing mTOR interacting protein (DEPTOR). It functions as an ATP and amino acid sensor to balance nutrient availability and cell growth, and the activation of mTORC1 inhibits autophagy (Mizushima et al., 2010). ULK1 is phosphorylated on serine 637 and 757 sites by mTOR in nutrient-rich conditions, inhibiting ULK1 activation by disrupting its binding to AMPK (Hosokawa et al., 2009; Mizushima et al., 2010). Conversely, AMPK regulates cellular metabolism to maintain energy homeostasis and promotes autophagy. Several studies have confirmed the positive regulation of ULK1 activity through AMPK-dependent phosphorylation. The S555 site of ULK1 is one of the major AMPK-dependent phosphorylation sites. In addition, several other sites of AMPK-dependent phosphorylation have been identified, such as S317, S467, T574, S637, and S777 (Egan et al., 2011; Kim et al., 2011). Among them, S317 and S777 are known to regulate the kinase activity of ULK1. S467, S555, and T574 are sites responsible for regulating mitochondrial homeostasis during starvation. S637 is the site where both mTORC1 and AMPK phosphorylate.

The attachment of O-linked N-acetylglucosamine (O-GlcNAcylation) is the covalent attachment of N-acetylglucosamine (GlcNAc) sugars to serine or threonine residues of protein substrates. It is catalyzed by a single enzyme, O-linked N-acetylglucosamine transferase (OGT), which transfers N-acetylglucosamine from uridine diphosphate (UDP)-GlcNAc to protein

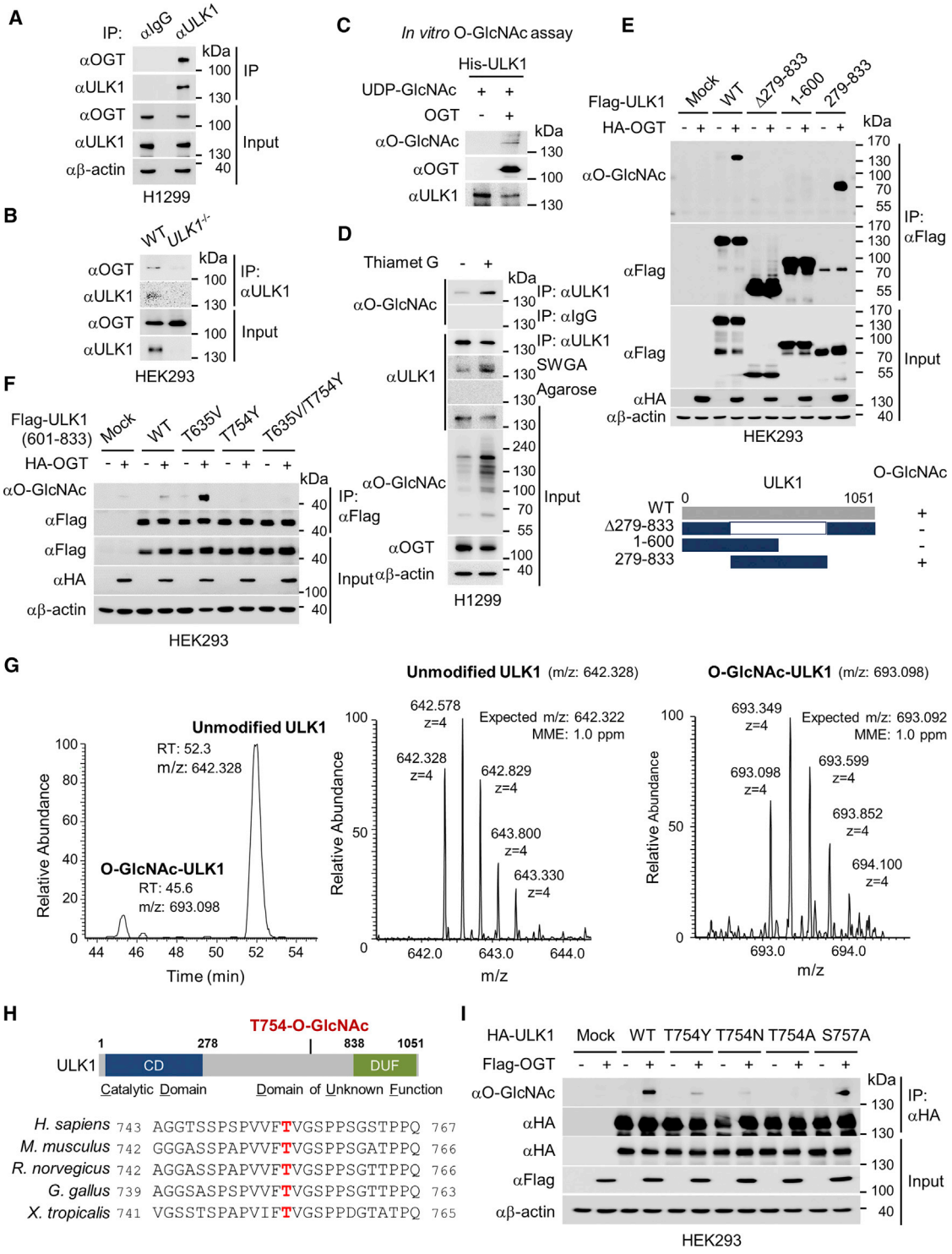

Figure 1. ULK1 Is O-GlcNAcylated by OGT on the Threonine 754 Site

(A) Co-immunoprecipitation of endogenous ULK1 with OGT in H1299 cells.

(B) Co-immunoprecipitation assay between ULK1 and OGT in WT or *ULK1*$^{-/-}$ HEK293 cells.

(C) Detection of ULK1 O-linked N-acetylglucosamine (O-GlcNAcylation) after *in vitro* O-GlcNAcylation assay.

(D) H1299 cells were treated with OGA inhibitor, Thiamet G (1 μM), followed by either pull down of O-GlcNAcylated proteins using succinyl wheat germ agglutinin (SWGA) or immunoprecipitation to detect ULK1 O-GlcNAcylation.

(E) ULK1 WT or deletion mutants, including Δ279–833, 1–600, and 279–833 aa, were tested for O-GlcNAcylation.

(legend continued on next page)

substrates. A single enzyme, known as O-GlcNAcase (OGA), rapidly removes the O-GlcNAcylation from protein substrates (Slawson and Hart, 2011; Vocadlo, 2012). These two opposing enzymes dynamically alter the posttranslational modification state and protein functions in response to various signals and cellular processes. OGT is enriched in the nucleus, yet it is also present in the cytosol (Zeidan and Hart, 2010). Insights into the function of OGT has more extensively come from studies focusing on O-GlcNAcylation of nuclear proteins such as histone H2B, histone-modifying enzymes such as EZH2 and HDAC1, and transcription factors such as Oct4 and Sox2 (Chen et al., 2013; Chu et al., 2014; Jang et al., 2012; Zhu et al., 2016).

There has been speculation that OGT may work closely with phosphatases since O-GlcNAcylation and phosphorylation share the same target residues serine and threonine, and therefore are most likely antagonistic to each other, such as in the cases of the CRTC2, p53, and CK2 proteins (Cheng and Hart, 2001; Chou et al., 1995; Dentin et al., 2008; Du et al., 2001; Tarrant et al., 2012; Yang et al., 2006). In support of this idea, OGT and phosphatases such as protein phosphatase 1β (PP1β) and PP1γ have been co-purified (Wells et al., 2004), although common targets of OGT and such phosphatases have not been identified thus far. It is notable that while kinases regulating ULK1 phosphorylation are well documented, the only phosphatase that has been reported is PP2A, which dephosphorylates ULK1 on the serine 637 site (Wong et al., 2015).

ULK1 regulates localization of a class III phosphatidylinositol 3 (PI3) kinase called VPS34, which phosphorylates the 3′ position of the phosphatidylinositol to produce PI(3) phosphate (PI(3)P), a key molecular marker for intracellular trafficking and autophagosome formation (Backer, 2008; Hara et al., 2008; Itakura and Mizushima, 2010). VPS34 is the only PI3 kinase in yeast and is essential for protein sorting to the vacuole via the endolysosomal pathway by producing PI(3)P (Backer, 2016; Schu et al., 1993). PI(3)P is localized to the endosomal compartment and is required for recruitment of downstream factors that contain PI(3)P-binding domains (Misra et al., 2001). VPS34 exists in different complexes and is involved in a variety of cellular functions such as multivesicular body pathway, retrograde trafficking from endosomes to the Golgi, phagosome maturation, and autophagy (Backer, 2008). It forms a stable complex with VPS15. VPS15 can also associate with Beclin1, which serves as a binding partner for several proteins that either promote (i.e., ATG14L, UVRAG, Bif1, and AMBRA-1) or inhibit (i.e., Bcl2, BclxL, and Rubicon) the autophagic function of VPS34 (Itakura et al., 2008; Liang et al., 2006; Matsunaga et al., 2009; Pattingre et al., 2009; Sun et al., 2008; Takahashi et al., 2007; Zalckvar et al., 2009; Zhong et al., 2009). In particular, ATG14L functions as a positive regulator of autophagosome formation because it determines the localization of VPS34, and the association with VPS34 complex is a prerequisite for the activation of VPS34 lipid kinase activity via AMPK (Kim et al., 2013; Matsunaga et al., 2009). However, little has been investigated regarding the mechanism of how ATG14L associates with the VPS34-Beclin1 complex.

Here, we provide evidence that ULK1 is O-GlcNAcylated by OGT on the T754 site during glucose starvation. ULK1 O-GlcNAcylation is crucial for the proper activation of VPS34 via ATG14L, the step that is essential for PI(3)P production, phagophore formation, and subsequent autophagy initiation.

RESULTS

ULK1 Is O-GlcNAcylated by OGT on the Threonine 754 Site

Since ULK1 functions as an important gatekeeper for the initiation of autophagy, we decided to look for possible upstream regulators of ULK1. We found that ULK1 and OGT interact with each other. A co-immunoprecipitation assay using antibody against ULK1 revealed that ULK1 bound to OGT at the endogenous expression level (Figure 1A). We generated *ULK1*$^{-/-}$ HEK293 cells using CRISPR/Cas9 and confirmed the specific interaction between ULK1 and OGT (Figure 1B). This led us to speculate that ULK1 may be a target of OGT. To verify whether O-GlcNAcylation occurs on ULK1, an *in vitro* OGT assay was performed. The introduction of OGT induced the O-GlcNAcylation of ULK1 (Figure 1C). Also, treatment of cells with the OGA inhibitor Thiamet G increased ULK1 O-GlcNAcylation, while the total protein level of ULK1 did not change (Figure 1D).

Next, we set out to identify the site of O-GlcNAcylation on ULK1. Several deletion mutants of ULK1 were tested for O-GlcNAcylation. Full-length Δ279–833, which has the 279–833 amino acid (aa) region deleted, 1–600 aa, and 279–833 aa were expressed in HEK293 cells and immunoprecipitated for O-GlcNAc band detection. ULK1 was O-GlcNAcylated only in the 601–833 aa region (Figure 1E). Although a recent study suggests that ULK1 is O-GlcNAcylated at two different sites, threonine 635 and threonine 754 (Ruan et al., 2017), in our context, threonine 754 was the major site of O-GlcNAcylation (Figure 1F). We went further to confirm the exact site of O-GlcNAcylation by electron transfer dissociation (ETD) mass spectrometric analysis and verified that ULK1 is O-GlcNAcylated on the threonine 754 site, which is well conserved across species (Figures 1G, 1H, and S1).

In addition, three different T754 mutants (T754A, T754N, and T754Y) of ULK1 were tested. We mutated threonine to alanine (A). Being close to the mTOR-mediated serine 757 (S757) phosphorylation site, we also decided to mutate T754 to asparagine (N) or tyrosine (Y), since these aas are conserved mTOR target motif sequences in the corresponding position (Hsu et al., 2011). We reasoned that mTOR-mediated phosphorylation on the S757 site should not be neglected because previous studies have shown that mTOR phosphorylates ULK1 in nutrient-rich conditions, while upon starvation, ULK1 phosphorylation by

(F) ULK1 WT or point mutants T635V, T754Y, and T635V/T754Y were pulled down with anti-FLAG antibody, and their O-GlcNAcylation band was detected.
(G) ETD mass spectrometry analysis revealed that the site of O-GlcNAcylation within ULK1 is threonine 754.
(H) The site of ULK1 O-GlcNAcylation is conserved throughout species.
(I) Threonine 754 mutated to tyrosine (Y), asparagine (N), or alanine (A), respectively. A residue other than T754, such as S757, was also mutated to alanine to validate the site of O-GlcNAcylation by co-immunoprecipitation.

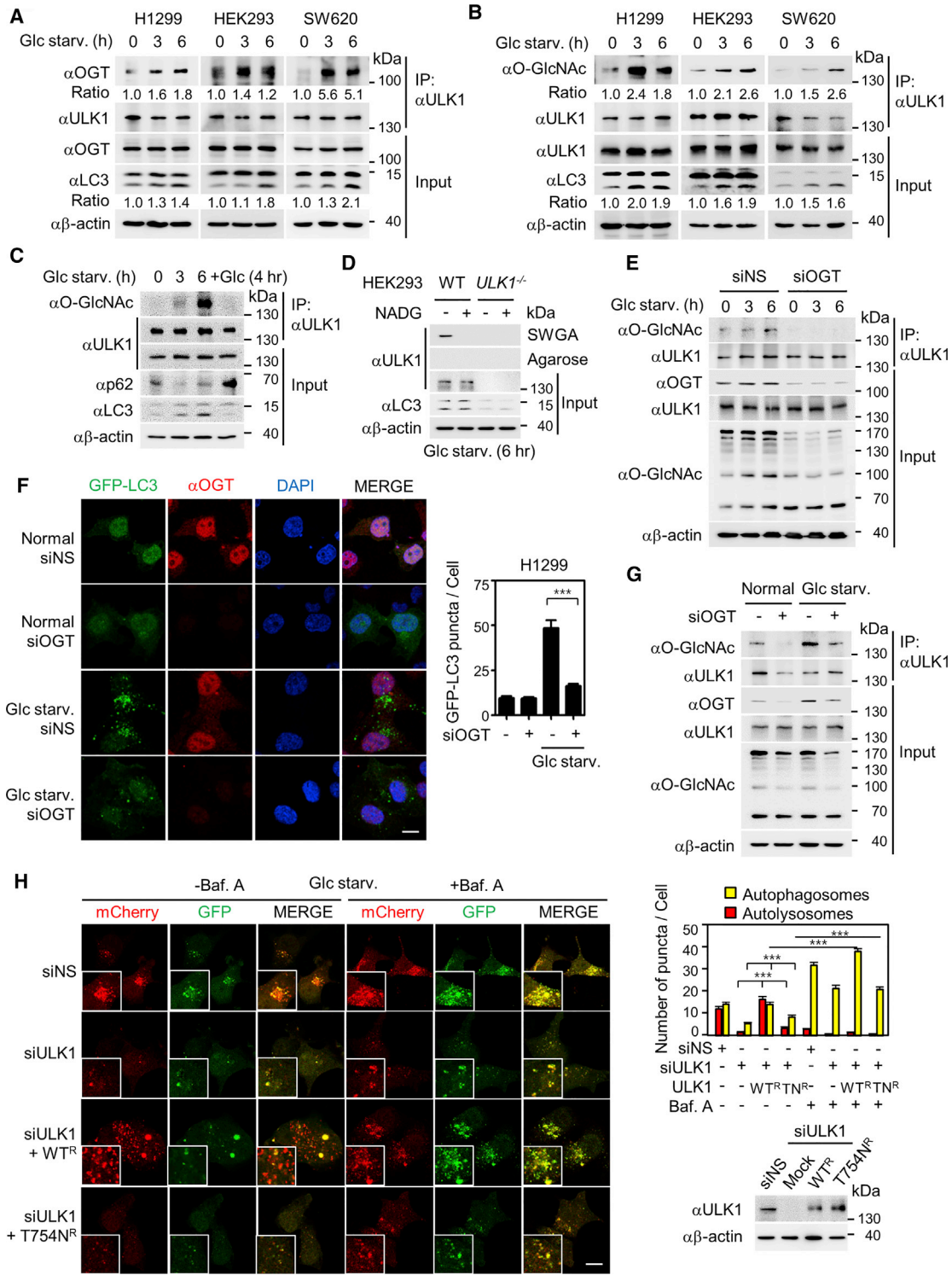

Figure 2. ULK1 O-GlcNAcylation Increases during Glucose Starvation

(A and B) Glucose starvation for the indicated times in H1299, HEK293, and SW620 cells. Samples were co-immunoprecipitated against anti-ULK1 antibody, and either endogenous OGT (A) or O-GlcNAcylation (B) levels were detected. The OGT/ULK1 or LC3-II/β-actin ratio is indicated.

(C) H1299 cells were glucose starved and resupplied for 4 hr before harvest.

(D) WT HEK293 cells were compared with *ULK1*$^{-/-}$ HEK293 cells to confirm ULK1-specific O-GlcNAcylation. SWGA beads were used to detect O-GlcNAcylation with or without N-acetyl-D-glucosamine (NADG), which mimics the free form of UDP-GlcNAc.

(legend continued on next page)

mTOR is diminished, which releases ULK1 from the inactive state (Kim et al., 2011). Therefore, several conserved-motif-based T754 mutants were made to ensure that mTOR-dependent phosphorylation occurs appropriately. In support of the ETD mass spectrometry data, co-immunoprecipitation and immunoblot analyses confirmed ULK1 O-GlcNAcylation on T754, since only WT but not T754Y, T754N, or T754A was O-GlcNAcylated (Figure 1I). We observed that the T754A mutant diminished S757 phosphorylation dynamics, which would affect the study on the interplay between O-GlcNAcylation by OGT and phosphorylation by mTOR (Figure S2). Therefore, we used the T754N mutant to explore the function of ULK1 O-GlcNAcylation thereafter.

Increased ULK1 O-GlcNAcylation Is Positively Correlated to Autophagosome Formation during Glucose Starvation

ULK1 activity largely depends on the availability of nutrients, and nutrient starvation conditions such as glucose starvation increase ULK1 activity (Kim et al., 2011; Shang and Wang, 2011). Therefore, we examined whether ULK1 and OGT interaction is affected by glucose starvation. Several different cell lines, including H1299, HEK293, and SW620, similarly showed increased binding between ULK1 and OGT upon glucose starvation (Figure 2A). In parallel, ULK1 O-GlcNAcylation levels increased during glucose starvation, which was in conjunction with increased LC3-phosphatidylethanolamine conjugate (LC3 II) conversion, a marker for autophagosomes and autolysosomes (Figure 2B), indicating that ULK1 O-GlcNAcylation has a positive correlation with autophagy occurrence in these cell lines. Furthermore, we reasoned that if glucose levels and ULK1 O-GlcNAcylation levels have inverse correlations, reversing glucose levels in the media would reverse ULK1 O-GlcNAcylation levels. Glucose starvation followed by glucose repletion resulted in the reversal of the modification, with a marked decrease in ULK1 O-GlcNAcylation levels after the restoration of glucose in the media (Figure 2C). We also confirmed that the ULK1 O-GlcNAcylation band disappeared when free N-acetyl-D-glucosamine ([NADG] mimics free UDP-GlcNAc) was added to the succinyl wheat germ agglutinin (SWGA) bead, but no such band appeared in the *ULK1*$^{-/-}$ HEK293 cells, indicating that the O-GlcNAcylation band is specific to ULK1 (Figure 2D).

We further examined whether knock down of OGT would result in the reduction of ULK1 O-GlcNAcylation levels and subsequently lead to the inhibition of autophagy. First, we confirmed dramatically decreased ULK1 O-GlcNAcylation levels over the course of starvation when OGT was knocked down by small interfering RNA (siRNA) (Figure 2E). Second, we used GFP-LC3 puncta as readout for autophagy occurrence and found that the number of GFP-LC3 puncta decreased when the OGT level was diminished, further indicating that OGT knockdown inhibits autophagosome formation (Figures 2F and 2G). To more precisely assess whether ULK1 O-GlcNAcylation modulates autophagosome formation, ULK1 was knocked down using siRNA, and then the siRNA-resistant ULK1 wild-type (WT) or T754N mutant was reconstituted. The mCherry-GFP-LC3 reporter was used to assess the overall number of LC3 puncta formations as well as autophagic flux. The GFP is attenuated in the acidic lysosomal environment, whereas the mCherry is not. This reporter allows the distinction between autophagosomes (GFP$^+$/mCherry$^+$ yellow puncta) and autolysosomes (GFP/mCherry$^+$ red puncta) to be made. The total numbers of both autophagosomes and autolysosomes were significantly reduced when the T754N mutant was reconstituted in contrast to WT reconstitution (Figure 2H), indicating that ULK1 O-GlcNAcylation positively regulates autophagosome formation. Bafilomycin A_1, which inhibits the fusion between autophagosomes and lysosomes, was used to assess autophagic flux. Treatment with bafilomycin A_1 resulted in significantly increased autophagosomes for both WT and T754N mutants. This increased number of nascent autophagosomes unable to fuse with lysosomes indicates that the major function of ULK1 O-GlcNAcylation is in the early regulation of autophagy progression (Figures 2H).

Dephosphorylation and O-GlcNAcylation on ULK1 Occur Sequentially

A previous study had quantified phosphorylation dynamics on 711 phosphopeptides through high-throughput mass spectrometric analyses (Wang et al., 2008). Elevated O-GlcNAcylation resulted in reduced phosphorylation on 280 sites and caused increased phosphorylation on 148 sites. The crosstalk between these two abundant modifications may have arisen by both steric competition for occupancy at the same or adjacent sites and each modification regulating the other's enzymatic machinery. Therefore, we decided to examine whether this crosstalk between O-GlcNAcylation and phosphorylation applies to ULK1, since it has been reported that ULK1 is phosphorylated by mTOR on S757 in nutrient-rich conditions (Hwang et al., 2017; Kim et al., 2011). S757 is only three aas away from the O-GlcNAcylation site, and this phosphorylation is known to be significantly diminished during nutrient starvation (Kim et al., 2011). We observed dephosphorylation of ULK1 on S757 simultaneously occurring with O-GlcNAcylation on T754 (Figure 3A),

(E) Knock down of nonspecific (siNS) or OGT (siOGT), followed by glucose starvation for the indicated hours.
(F) Representative image of immunocytochemistry after knock down of nonspecific (siNS) or endogenous *OGT* (siOGT) (red) and overexpression of GFP-LC3 (green) for the quantification of LC3 puncta in H1299 cells. Nuclei visualized by DAPI staining (blue). Similar results were obtained in three independent experiments performed using the same conditions. Scale bar, 10 μm. The p value was calculated by t test (***$p < 0.0001$). Data are expressed as means ± SEMs.
(G) Immunoprecipitation assay was performed in parallel with the immunocytochemistry samples to confirm efficient knock down of OGT and subsequent reduction in ULK1 O-GlcNAcylation.
(H) Representative image of immunocytochemistry after knockdown of endogenous *ULK1* (siULK1) and reconstitution with WT (WT^R) or T754N (T754N^R) siRNA-resistant ULK1 in H1299 cells. All of the cells were glucose starved to induce autophagy. Treatment of cells with either vehicle or 40 nM of bafilomycin A_1 for 2 hr was done before fixation. Similar results were obtained in three independent experiments performed using the same conditions. Scale bar, 10 μm. The p value was calculated by one-way ANOVA (***$p < 0.0001$). Data are expressed as means ± SEMs. Immunoblot showing knockdown and reconstitution efficiency of ULK1 WT or T754N mutants in H1299 cells in parallel with the immunocytochemistry experiment.

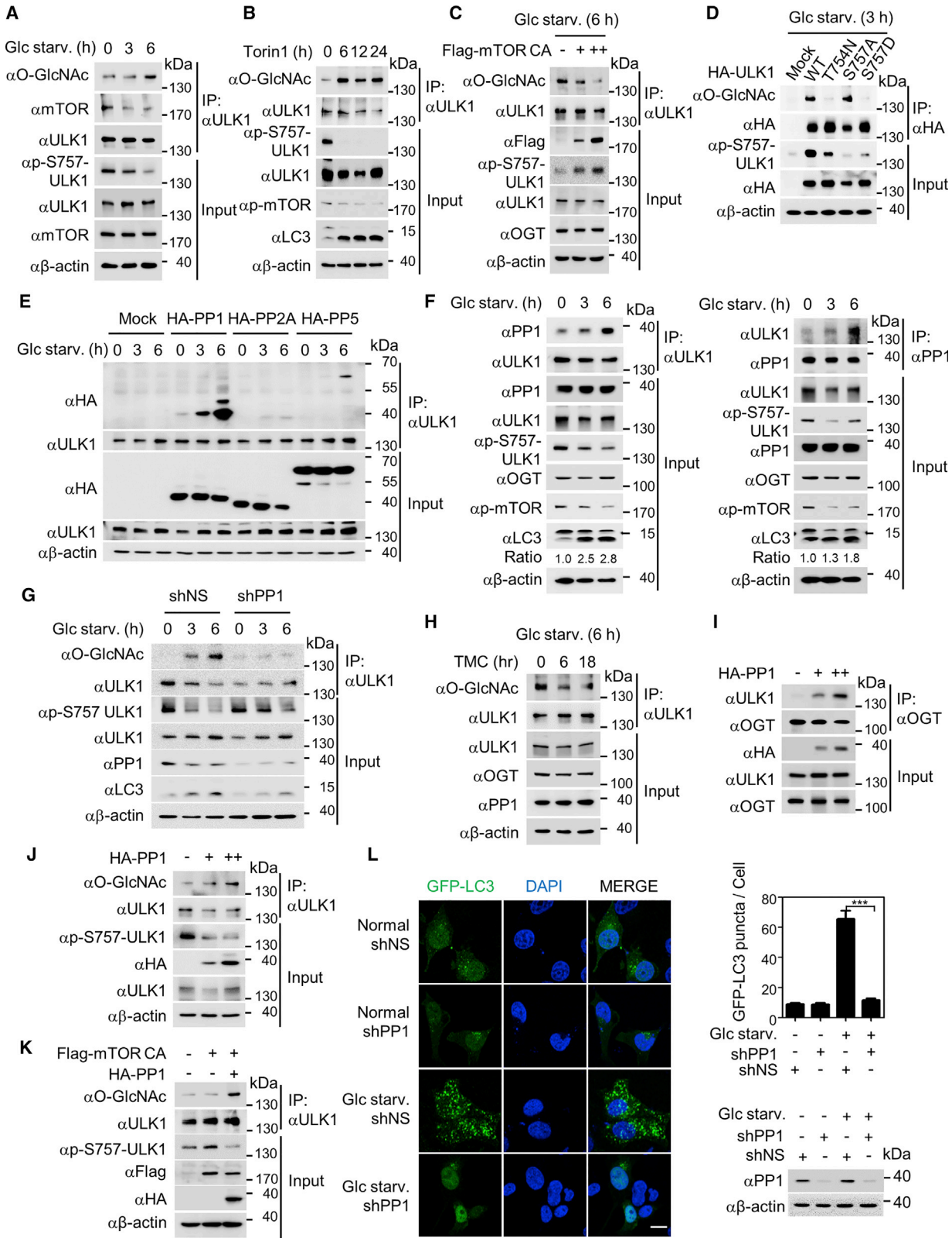

(legend on next page)

indicating that these two different modifications may be able to crosstalk with each other. We also noticed that binding between ULK1 and mTOR decreased during glucose starvation (Figure 3A).

Based on the preceding evidence, we set out to test whether there is a correlation between O-GlcNAcylation and phosphorylation on ULK1. ULK1 phosphorylation by mTOR is known to negatively regulate ULK1 activity when sufficient nutrients are available. Therefore, we treated cells with Torin 1 to inhibit mTOR activity and found that ULK1 phosphorylation by mTOR on S757 decreased as O-GlcNAcylation on T754 increased (Figure 3B). Next, we reasoned that overexpression of the constitutively active form of mTOR would sufficiently reverse O-GlcNAcylation during glucose starvation for this negative correlation to be valid. The constitutively active mutant of mTOR (mTOR CA) has its four sites mutated (I2017T, V2198A, L2216H, and L2260P) (Das et al., 2012). Using mTOR CA, we verified that O-GlcNAcylation of ULK1 was reversed by the overexpression of this mutant. ULK1 O-GlcNAcylation was dose dependently decreased, while adjacent phosphorylation dose dependently increased by mTOR CA overexpression (Figure 3C), indicating the alternative and reversible aspects of ULK1 T754 O-GlcNAcylation and S757 phosphorylation. In addition, WT and mutant forms of ULK1 were tested for O-GlcNAcylation and phosphorylation after glucose starvation. As expected, both the T754N mutant and the S757D (phospho-S757 mimic) mutant failed to obtain O-GlcNAcylation, while both WT and S757A were capable of being O-GlcNAcylated (Figure 3D). These results provide evidence for consecutive dephosphorylation and O-GlcNAcylation during glucose starvation. In other words, O-GlcNAcylation occurrence after ULK1 phosphorylation on S757 is significantly diminished.

Next, we predicted that there would be an active phosphatase responsible for the dephosphorylation of ULK1. We found PP1 to be the active phosphatase, whose interaction with ULK1 was significantly stronger than other phosphatases such as PP2A and PP5 during glucose starvation (Figure 3E). PP5 knock down resulted in increased LC3 II levels in contrast to PP1, supporting the idea that PP1, but not PP5, would be a strong candidate phosphatase (Figure S3). Although its protein level remained stable, PP1 showed increased binding to ULK1 during glucose starvation (Figure 3F). As the binding increased, ULK1 phosphorylation on S757 decreased, indicating the possible involvement of PP1 in mediating the dephosphorylation of ULK1 on S757. Furthermore, the interaction between ULK1 and PP1 was visualized by immunocytochemistry. Under nutrient-rich conditions, ULK1 and PP1 did not colocalize in the cells, whereas during glucose starvation, their colocalization was significantly increased (Figure S4). Following the observation that ULK1 and PP1 colocalize, PP1 was knocked down to test whether PP1 is essential for ULK1 O-GlcNAcylation to occur. The absence of PP1 led to a dramatic decrease in ULK1 O-GlcNAcylation during glucose starvation (Figure 3G).

We next determined whether this dephosphorylation event occurs specifically by PP1 using a PP1-specific inhibitor, tautomycetin (TMC). The treatment of glucose-starved cells with TMC resulted in significantly reduced ULK1 O-GlcNAcylation (Figure 3H), indicating that the dephosphorylation event is required for O-GlcNAcylation to occur during glucose starvation. In addition, PP1 overexpression increased the binding between ULK1 and OGT (Figure 3I). As a result, ULK1 O-GlcNAcylation increased dose dependently via the overexpression of PP1, while adjacent phosphorylation on S757 was dramatically decreased (Figure 3J), indicating that the dephosphorylation event by PP1 precedes binding between ULK1 and OGT and subsequent ULK1 O-GlcNAcylation. These results provided further evidence that the withdrawal of mTOR from ULK1 during glucose starvation is not sufficient for efficient ULK1 O-GlcNAcylation and that an active dephosphorylation event by PP1 is pivotal for proper interaction between ULK1 and OGT and subsequent O-GlcNAcylation. Also, the overexpression of PP1 was sufficient to overcome the suppression of ULK1 O-GlcNAcylation by mTOR, as was indicated by reversed O-GlcNAcylation and phosphorylation states (Figure 3K). Based on these results, we predicted that knock down of endogenous *PP1* would inhibit autophagosome formation in parallel with the knock down of endogenous OGT, as shown in Figure 2F. As expected, knock down of *PP1* resulted in the dramatically reduced number of GFP-LC3 puncta during glucose starvation (Figure 3L). These data not only represent the close relation between ULK1 and PP1 but also indicate that PP1 colocalizes with ULK1

Figure 3. Dephosphorylation and O-GlcNAcylation on ULK1 Occurs Sequentially

(A) Detection of ULK1 T754 O-GlcNAcylation and S757 phosphorylation after the indicated hours of glucose starvation in H1299 cells.

(B) Detection of ULK1 O-GlcNAcylation and S757 phosphorylation after treatment of H1299 cells with mTOR inhibitor Torin 1 for the indicated hours.

(C) Overexpression of mTOR constitutively active mutant (mTOR CA), followed by detection of ULK1 O-GlcNAcylation. Cells were glucose starved for 6 hr to induce ULK1 O-GlcNAcylation before harvest.

(D) Overexpression of hemagglutinin (HA)-tagged ULK1 WT and mutants T754N, S757A, and S757D in HEK293 cells, followed by glucose starvation, immunoprecipitation using anti-HA antibody, and immunoblot analysis against the indicated antibodies.

(E) Comparison of binding between ULK1 and phosphatases (PP1, PP2A, and PP5) during glucose starvation in HEK293 cells.

(F) Co-immunoprecipitation of endogenous ULK1 and PP1 after the indicated hours of glucose starvation in H1299 cells.

(G) Immunoprecipitation assay detecting ULK1 O-GlcNAcylation in H1299 cells when PP1 was knocked down using shRNA and underwent glucose starvation for the indicated hours.

(H) Tautomycetin (TMC) treatment (10 nM) for the indicated hours, followed by the detection of ULK1 O-GlcNAcylation in H1299 cells.

(I) Co-immunoprecipitation of ULK1 and OGT after the overexpression of PP1 in HEK293 cells.

(J) Overexpression of PP1, followed by detection of ULK1 O-GlcNAcylation and S757 phosphorylation in H1299 cells.

(K) Detection of ULK1 O-GlcNAcylation and S757 phosphorylation when mTOR CA is expressed in the absence or presence of PP1 in H1299 cells.

(L) Representative image of immunocytochemistry showing GFP-LC3 (green) puncta in H1299 cells with or without endogenous *PP1* knockdown using shRNA. Nuclei visualized by DAPI staining (blue). Similar results were obtained in three independent experiments performed using the same conditions. Scale bar, 10 μm. The p value was calculated by t test (***$p < 0.0001$). Data are expressed as means ± SEMs. Immunoblot analysis showing knockdown efficiency of endogenous *PP1* in parallel with the immunocytochemistry experiment.

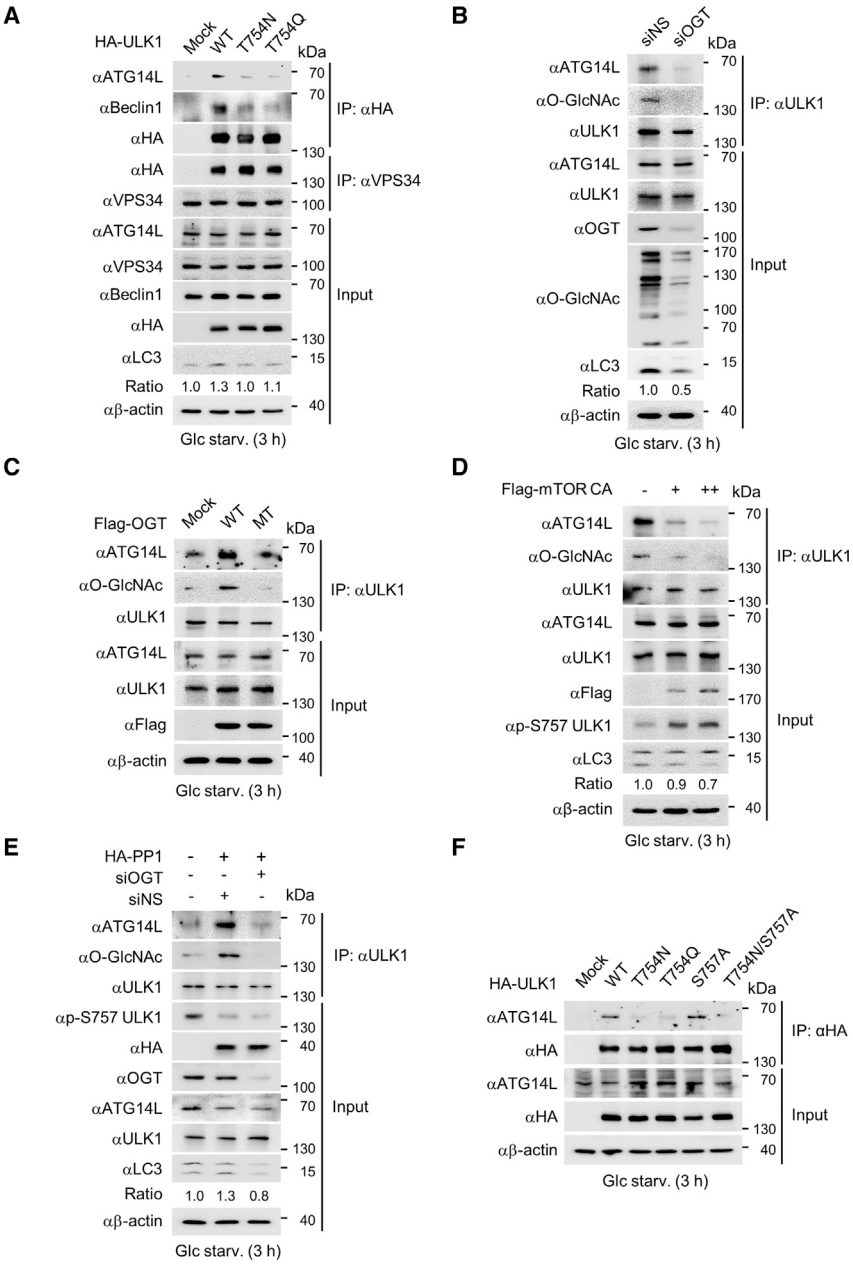

Figure 4. ULK1 O-GlcNAcylation Is Crucial for Activating VPS34 via ATG14L during Autophagy Initiation

(A) Co-immunoprecipitation of ULK1 WT or T754N/T754Q mutants with endogenous ATG14L, Beclin1, and VPS34 in HEK293 cells after 3 hr of glucose starvation. Input was divided in half to perform two separate co-immunoprecipitation assays.

(B) Knock down of endogenous OGT, followed by 3 hr of glucose starvation and co-immunoprecipitation with anti-ULK1 antibody, followed by immunoblot analysis with anti-ATG14L, anti-O-GlcNac, and ULK1 antibodies in H1299 cells.

(C) Co-immunoprecipitation of endogenous ULK1 and ATG14L when OGT WT mutant or enzymatic dead mutant is overexpressed in HEK293 cells.

(D) Overexpression of mTOR CA mutant in HEK293 cells upon glucose starvation for 3 hr. A co-immunoprecipitation assay was performed with anti-ULK1 antibody, followed by immunoblot analysis using the indicated antibodies.

(E) Overexpression of PP1, followed by knock down of OGT in H1299 cells. Immunoprecipitation was performed using anti-ULK1 antibody, followed by immunoblotting using the indicated antibodies. Glucose starvation was provided for 3 hr before harvest.

(F) ULK1 WT, T754N, T754Q, S757A, and T754N/S757A mutants were reconstituted in *ULK1*$^{-/-}$ HEK293 cells. Glucose starvation was provided for 3 hr before harvest.

to ensure that ULK1 remains dephosphorylated throughout starvation, thereby serving as a gatekeeper between O-GlcNAcylation by OGT and phosphorylation by mTOR.

ULK1 O-GlcNAcylation Is Crucial for Activating VPS34 via ATG14L during Autophagy Initiation

Since the T754 O-GlcNAcylation site is structurally within the regulatory region of ULK1, this modification may alter its kinase activity. Therefore, we performed an *in vitro* kinase assay using ATG13 as a substrate and found that T754N and T754A mutants exhibited little or no change in kinase activity on ATG13 (Figure S5A). To exclude the possibility that the mutation results in structural defects, we performed immunoprecipitation of WT and mutant ULK1 with ATG13. There was no significant defect in the ability to bind ATG13 (Figure S5B). Next, we decided to explore other aspects of ULK1 function that would be affected by O-GlcNAcylation, such as protein-protein interaction. We explored the binding affinity with known ULK1 targets such as ATG14L and VPS34. Being a positive regulator of autophagosome formation and an important regulator of VPS34 complex, ATG14L binding to ULK1 T754N and T754Q was dramatically decreased when compared to ULK1 WT (Figure 4A). T754Q mutant was used as one of the conserved mTOR target motif-based T754 mutants in addition to T754N. Knock down of OGT significantly decreased the interaction between ULK1 and ATG14L (Figure 4B). Based on our observation that ULK1 O-GlcNAcylation is required for proper binding to ATG14L, we examined whether overexpression of either WT or the enzymatically dead mutant of OGT would alter the binding between ULK1 and ATG14L. OGT WT, but not the mutant, caused increased binding between ULK1 and ATG14L, confirming the importance of O-GlcNAcylation in facilitating their interaction (Figure 4C). In addition, since overexpression of mTOR CA led to decreased O-GlcNAcylation in Figure 3C, we reasoned that this would also lead to reduced ULK1-ATG14L binding. ULK1-ATG14L binding decreased, as opposed to S757 phosphorylation, which increased due to mTOR activity (Figure 4D).

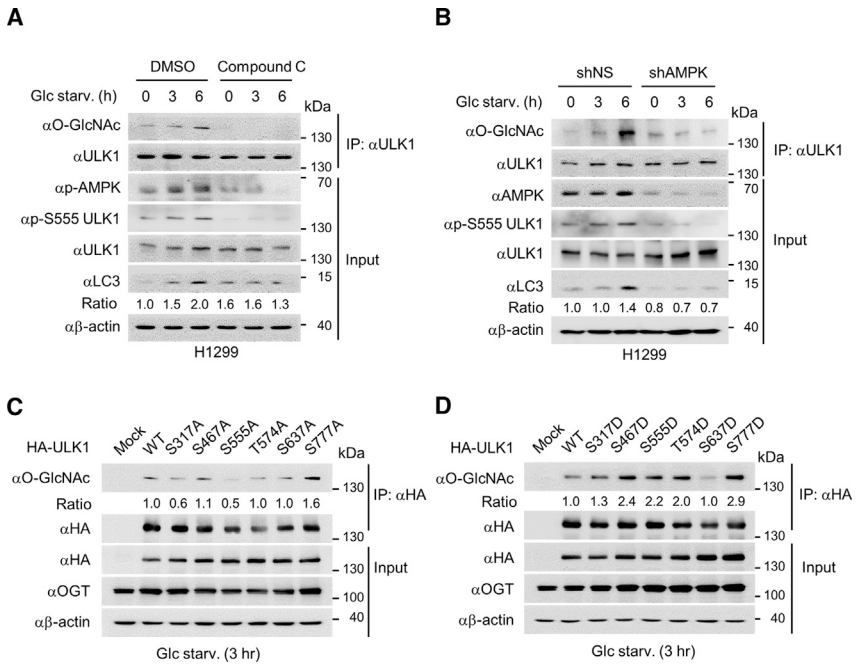

Figure 5. Phosphorylation by AMPK Precedes ULK1 O-GlcNAcylation

(A and B) H1299 cells were treated with Compound C (10 μM) (A) or knocked down by AMPKα shRNA (B) during glucose starvation for the indicated hours. Immunoprecipitation was performed with anti-ULK1 antibody, followed by immunoblot analysis using the indicated antibodies.

(C and D) HA-tagged ULK1 WT, S317A, S467, S555A, T574A, S637A, and S777A mutants (C) or HA-tagged ULK1 WT, S317D, S467D, S555D, T574D, S637D, and S777D mutants (D) were overexpressed with OGT in HEK293 cells and provided glucose starvation for 3 hr before harvest. Immunoprecipitation was performed using anti-HA antibody followed by immunoblotting using the indicated antibodies. The O-GlcNAc/HA ratio is indicated.

One may argue the legitimacy of O-GlcNAcylation because the dephosphorylation event may be sufficient to trigger the interaction between ULK1 and ATG14L. To test this possibility, we overexpressed PP1 to dephosphorylate ULK1 and then knocked down OGT so that ULK1 remained dephosphorylated and deO-GlcNAcylated. The interaction between ULK1 and ATG14L diminished when OGT was knocked down, indicating that O-GlcNAcylation has its own function besides crosstalk with the adjacent phosphorylation (Figure 4E). We continued to confirm the hypothesis by comparing ULK1 WT with O-GlcNAc mutants T754N and T754Q, phosphorylation mutant S757A, and double mutant T754N/S757A. T754N/S757A mutant was included because this form would represent dephosphorylated and deO-GlcNAcylated state of ULK1. Only WT and S757A mutants were able to bind ATG14L, indicating that dephosphorylated and deO-GlcNAcylated ULK1 showed attenuated binding to ATG14L (Figure 4F). In summary, O-GlcNAcylation requires the dephosphorylation event, yet it confers onto ULK1 its own function, which is the interaction with ATG14L.

Phosphorylation by AMPK Occurs Before ULK1 O-GlcNAcylation

Based on the previous studies that showed that AMPK and mTORC1 are antagonistic to each other in the function of ULK1, we wondered where O-GlcNAcylation would fit. We treated cells with an AMPK inhibitor, Compound C, during glucose starvation and observed dramatically decreased O-GlcNAcylation and AMPK-dependent S555 phosphorylation on ULK1 (Figure 5A). This result supports the idea that O-GlcNAcylation occurs after AMPK phosphorylates ULK1 and that this phosphorylation is required for O-GlcNAcylation to occur. To further verify this hypothesis, we transiently knocked down *AMPKα* using small hairpin RNA (shRNA) in glucose-starved cells. In parallel with Compound C treatment, *AMPK* knockdown also abolished both ULK1 O-GlcNAcylation and AMPK-dependent S555 phosphorylation (Figure 5B).

However, it is possible that since AMPK has been inhibited or knocked down, the entire autophagic process may have been shut down, and OGT may have been affected by it. To exclude such a possibility, we mutated AMPK-dependent phosphorylation sites of ULK1, which are S317, S467, S555, T574, S637, and S777, to alanine (SA) to determine whether this mutation results in the reduction of O-GlcNAcylation. Two SA mutants showed significantly diminished O-GlcNAcylation, indicating that AMPK-dependent phosphorylation on ULK1 S317 and S555 occurs before O-GlcNAcylation on T754 (Figure 5C). Conversely, the six sites were mutated to aspartic acid (SD) to mimic constitutive phosphorylation, and the SD mutation of S317 and S555 showed increased O-GlcNAcylation bands in contrast to the SA mutation of them (Figure 5D). This also indicates that phosphorylation of ULK1 by AMPK occurs before ULK1 O-GlcNAcylation and that it possibly has positive effects on ULK1 O-GlcNAcylation. These results demonstrate that there is a sequence of modification steps on ULK1 during glucose starvation. Dephosphorylation by PP1 and phosphorylation by AMPK are followed by ULK1 O-GlcNAcylation by OGT, and these series of events lead to the interaction of ULK1 and ATG14L.

Interplay between Dephosphorylation and O-GlcNAcylation of ULK1 Governs the Autophagy Initiation Process

Based on the evidence that PP1 upregulates ULK1 O-GlcNAcylation and that O-GlcNAcylation is required for the ULK1-ATG14L interaction, we tested whether the interaction between ATG14L and ULK1 is affected by the dephosphorylation of ULK1 on S757 by PP1. The overexpression of PP1 increased the binding between ULK1 and ATG14L dose dependently during glucose starvation (Figure 6A). Since ULK1 is a serine/threonine kinase and components of the VPS34 complex such as VPS34 and Beclin1 are phosphorylated by ULK1, we

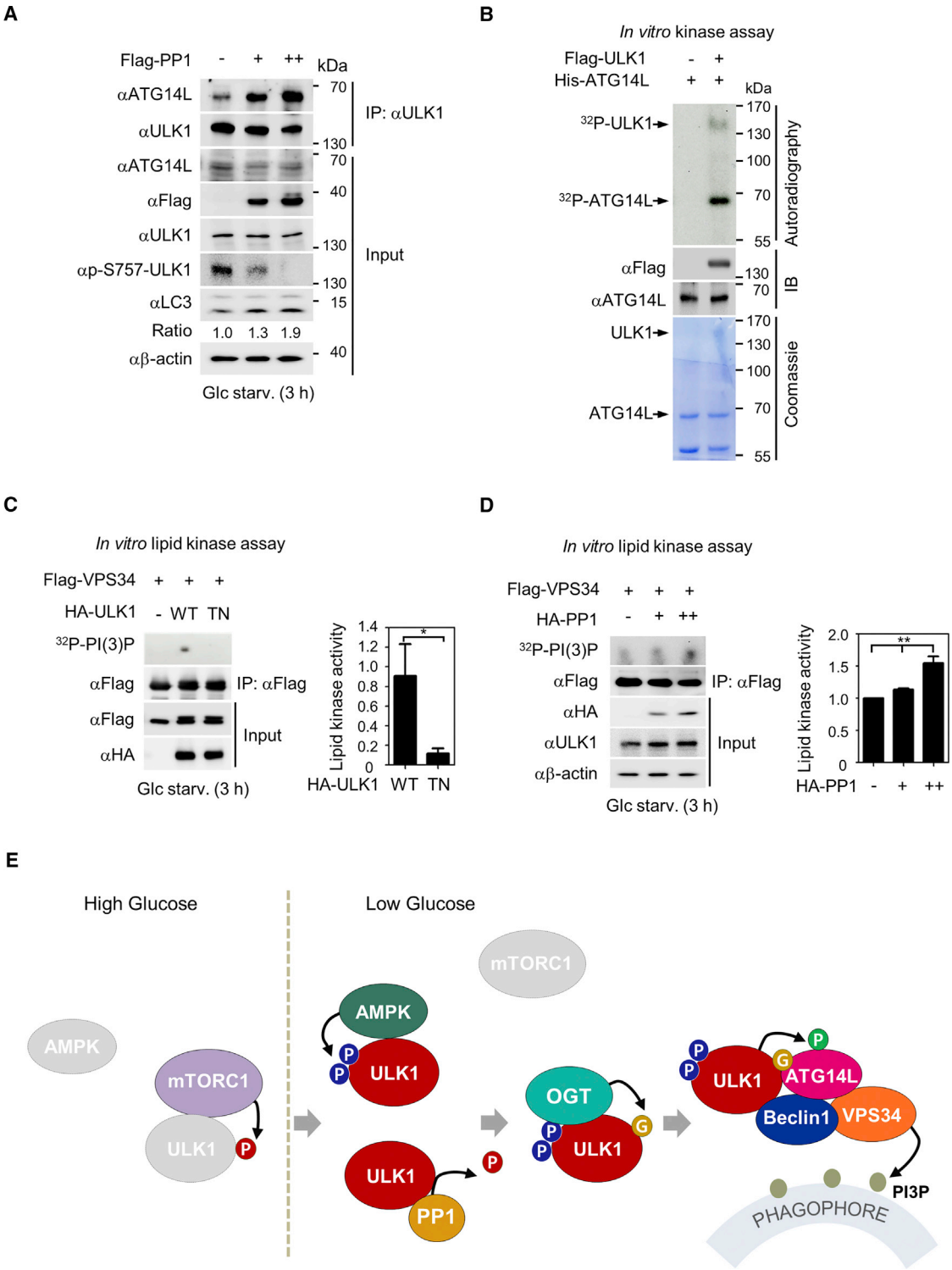

Figure 6. Interplay between Dephosphorylation and O-GlcNAcylation of ULK1 Governs the Autophagy Initiation Process

(A) Overexpression of PP1 in H1299 cells upon glucose starvation for 3 hr. Co-immunoprecipitation was performed using anti-ULK1 antibody, followed by immunoblot analysis with the indicated antibodies.

(B) *In vitro* kinase assay. FLAG-ULK1 overexpressing cells were glucose starved for 3 hr and harvested for pull-down assay with anti-FLAG M2 beads. The isolated protein was eluted with FLAG peptide for the *in vitro* kinase assay. *Escherichia coli* strain M13pRep was used for amplifying and purifying pQE-His-ATG14L protein by nickel-nitrilotriacetic acid (Ni-NTA) pull-down. ^{32}P was used for detecting phosphorylation on ATG14L.

(legend continued on next page)

hypothesized that the interaction between ULK1 and ATG14L would also induce phosphorylation of the VPS34 complex component ATG14L. This possibility was in line with the previous report that ATG14L phosphorylation mimics nutrient deprivation by stimulating the kinase activity of the VPS34 complex and facilitates the formation of phagophores and autophagosomes (Park et al., 2016). To visualize the phosphorylation of ATG14L by ULK1, an *in vitro* kinase assay was performed. The phosphorylated form of ATG14L was detected, and ULK1 phosphorylation was also detected since it has auto-kinase activity by autoradiography (Figure 6B). Therefore, using this method, we verified that ULK1 can induce the phosphorylation of ATG14L.

It has been shown that in the presence of ATG14L, the VPS34 complex is activated by AMPK, whereas in the absence of ATG14L, the VPS34 complex is inhibited by AMPK (Kim et al., 2013). Based on this information, we hypothesized that the failure of ULK1-ATG14L binding would result in the failure of VPS34 lipid kinase activation. An *in vitro* VPS34 lipid kinase assay confirmed that the reconstitution of *ULK1*$^{-/-}$ HEK293 cells with the ULK1 WT mutant but not the T754N mutant induced VPS34 lipid kinase activity (Figure 6C). Another *in vitro* VPS34 lipid kinase assay was performed by overexpressing PP1 in HEK293 cells. VPS34 activity was dose dependently induced, as shown by the increased level of ^{32}P-PI(3)P (Figure 6D).

Given that VPS34 can be involved in non-autophagy processes, we set out to further verify whether the ULK1 O-GlcNAc mutant disrupts an autophagy-specific function of VPS34. Members of the human tryptophan-aspartic acid (WD)-repeat protein interacting with phosphoinositides (WIPI) family play an important role in recognizing PI(3)P at the phagophore, and they function as autophagy-specific PI(3)P-binding effectors (Proikas-Cezanne et al., 2015). Since WIPI localization is dependent on VPS34 activity and PI(3)P, WIPI puncta formation was compared between ULK1 WT- and T754N-reconstituted cells. When undergoing glucose starvation, ULK1 T754N-reconstituted cells exhibited significantly less WIPI puncta than did ULK1 WT-reconstituted cells (Figure S6). This result indicates that VPS34 activity, which is indicated by WIPI puncta formation, depends on ULK1 O-GlcNAcylation. These data highlight that ULK1 O-GlcNAcylation is important for the induction of VPS34 lipid kinase activity by ATG14L, which is critical for PI(3)P conversion and phagophore formation.

DISCUSSION

Our study demonstrates that the initiation of autophagy during glucose starvation is critically regulated by a series of modification steps in ULK1, including dephosphorylation by PP1 and phosphorylation by AMPK, leading to O-GlcNAcylation by OGT. Moreover, we identify the site of ULK1 O-GlcNAcylation triggered by the starvation signal and exemplify how ULK1 O-GlcNAcylation is crucial for autophagosome formation by inducing the lipid kinase activity of the VPS34 via ATG14L (Figure 6E).

Previous studies have reported that OGT is recruited to sites of PI(3)P formation during growth factor signaling, suggesting that many signaling cascades triggered by phosphoinositide 3-kinase (PI3K) are likely to be influenced by O-GlcNAcylation (Yang et al., 2008). By analogy from its recruitment to PI(3)P in the plasma membrane, OGT has been predicted to be directly recruited to the forming autophagosome (Hanover et al., 2010). We identified a specific target of OGT at the pre-autophagosomal structure, ULK1, whose localization to the phagophore recruits ATG14L to induce VPS34, a type III PI3K, and allows the formation of PI(3)P. Generation of PI(3)P at the phagophore by VPS34 is a critical event during pre-autophagosomal structure formation. Two independent studies indicate that ATG14L positively regulates autophagy by promoting double-membrane formation during autophagy and that ATG14L deficiency causes defects in autophagosome formation (Matsunaga et al., 2009; Zhong et al., 2009). Moreover, the activity of ATG14L-containing VPS34 complex is strongly dependent on ULK1, yet a detailed regulatory mechanism has not been fully investigated. In the present study, we provide evidence that ULK1 O-GlcNAcylation exerts its function by upregulating VPS34 lipid kinase activity via increased binding between ULK1 and ATG14L.

Furthermore, we addressed how a phosphatase can mediate O-GlcNAcylation by demonstrating that PP1 dephosphorylates ULK1 on S757, which is in close proximity to the O-GlcNAcylation site T754. This may serve as a "priming event" for O-GlcNAcylation to occur during glucose starvation and may serve as an intermediary step between phosphorylation by mTOR and O-GlcNAcylation by OGT. Likewise, we speculate that there may be other common targets of PP1 and OGT during glucose starvation, since it has been reported that during glucose starvation, global O-GlcNAcylation levels rise in H1299 cells (Yi et al., 2012). Our findings strongly demonstrate that O-GlcNAcylation of ULK1 on the T754 site occurs to ensure the activation of VPS34 via increased binding to ATG14L for phagophore formation. Moreover, we found previously predicted yet never identified crosstalk between O-GlcNAcylation and dephosphorylation mediated by PP1 governing ULK1 function during autophagy initiation.

Phosphorylation of ULK1 on S317 and S555 by AMPK precedes ULK1 O-GlcNAcylation during glucose starvation. The phosphorylation status of other sites such as S467, T574, and S777 appears to have a minimal effect on ULK1 O-GlcNAcylation, while phosphorylation on S637 does not exert much influence on the status of ULK1 O-GlcNAcylation. During glucose starvation, mTOR is inhibited while AMPK is activated; therefore, during the early stages of autophagy, the net phosphorylation on the S637 site remains ambiguous (Shang and

(C and D) Lysates containing FLAG-VPS34 were subjected to pull-down assay with anti-FLAG M2 beads. The isolated protein was eluted with FLAG peptide, followed by *in vitro* lipid kinase assay. ^{32}P-PI(3)P production by VPS34 in response to ULK1 WT mutant or TN mutant overexpression (C) or PP1 overexpression (D) was measured using thin-layer chromatography (TLC), followed by autoradiography. Three independent experiments were performed and were analyzed for statistics. The p value was calculated by t test (*$p < 0.01$) or one-way ANOVA (**$p < 0.001$). Data are expressed as means ± SEMs.
(E) Schematic model of both dephosphorylation by PP1 and phosphorylation by AMPK events leading to O-GlcNAcylation by OGT on ULK1 during glucose starvation, and the consequential regulation of VPS34 activity via ATG14L and phagophore formation.

Wang, 2011). Moreover, the S757 site is phosphorylated solely by mTOR, but knock down of AMPK subunits or perturbations of AMPK activity by inhibitors may affect phosphorylation on S757 because AMPK inhibits mTOR during starvation. Further studies using these criteria are needed to validate the exact underlying mechanism.

Our study indicates that a series of posttranslational modifications of ULK1 during glucose starvation serves as a gatekeeper between pro-autophagic and anti-autophagic response, which is required for the decision-making process during autophagy. We predict that since autophagy is an energy-consuming process involving both short-term and long-term measures for cell survival, the cell may use a series of steps as checkpoints to determine whether the rest of the reactions should follow. Our data highlight the regulation of autophagy by crosstalk between dephosphorylation and O-GlcNAcylation during the initial stages of autophagy, offering therapeutic targets for autophagy-related diseases.

STAR★METHODS

Detailed methods are provided in the online version of this paper and include the following:

- KEY RESOURCES TABLE
- CONTACT FOR REAGENT AND RESOURCE SHARING
- EXPERIMENTAL MODEL AND SUBJECT DETAILS
  - Cell lines
- METHOD DETAILS
  - Cell culture
  - Generation of ULK1$^{-/-}$ cells using CRISPR/Cas9
  - LC-ETD-MS/MS analysis
  - Plasmids
  - Antibodies and reagents
  - Co-immunoprecipitation assays
  - Immunofluorescence microscopy
  - *In vitro* kinase assay
  - *In vitro* VPS34 lipid kinase assay
  - *In vitro* OGT assay
- QUANTIFICATION AND STATISTICAL ANALYSIS
- DATA AND SOFTWARE AVAILABILITY

SUPPLEMENTAL INFORMATION

Supplemental Information includes six figures and can be found with this article online at https://doi.org/10.1016/j.celrep.2018.11.042.

ACKNOWLEDGMENTS

FLAG-ncOGT and Thiamet G were kind gifts from Prof. Jin Won Cho (Yeonsei University, South Korea), and GFP-hLC3 was from Prof. Chanhee Kang (Seoul National University, South Korea). We thank members of the Epigenetic Code and Diseases Research Center for discussions and Seung Hyeun Ka for technical assistance. This work was supported by the Creative Research Initiatives Program (Research Center for Epigenetic Code and Diseases, NRF-2017R1A3B1023387 to S.H.B.); the Science Research Center Program (Cellular Heterogeneity Research Center, NRF-2016R1A5A1011974 to K.I.K., and Glycosylation Network Research Center, NRF-2016R1A5A1010764 to S.H.B.). IBS-R008-D1 (to J.-S.K.) from the National Research Foundation (NRF) was funded by the Korean government (the Ministry of Science and ICT).

AUTHOR CONTRIBUTIONS

K.E.P., K.I.K., and S.H.B. designed the research; K.E.P., C.R.K., and M.L. performed the research; J.-S.K. performed the mass spectrometric analysis; and K.E.P., K.I.K., and S.H.B. wrote the paper.

DECLARATION OF INTERESTS

The authors declare no competing interests.

Received: February 22, 2018
Revised: July 4, 2018
Accepted: November 9, 2018
Published: December 4, 2018

REFERENCES

Abada, A., and Elazar, Z. (2014). Getting ready for building: signaling and autophagosome biogenesis. EMBO Rep. *15*, 839–852.

Backer, J.M. (2008). The regulation and function of Class III PI3Ks: novel roles for Vps34. Biochem. J. *410*, 1–17.

Backer, J.M. (2016). The intricate regulation and complex functions of the Class III phosphoinositide 3-kinase Vps34. Biochem. J. *473*, 2251–2271.

Chen, Q., Chen, Y., Bian, C., Fujiki, R., and Yu, X. (2013). TET2 promotes histone O-GlcNAcylation during gene transcription. Nature *493*, 561–564.

Cheng, X., and Hart, G.W. (2001). Alternative O-glycosylation/O-phosphorylation of serine-16 in murine estrogen receptor beta: post-translational regulation of turnover and transactivation activity. J. Biol. Chem. *276*, 10570–10575.

Chou, T.Y., Hart, G.W., and Dang, C.V. (1995). c-Myc is glycosylated at threonine 58, a known phosphorylation site and a mutational hot spot in lymphomas. J. Biol. Chem. *270*, 18961–18965.

Chu, C.S., Lo, P.W., Yeh, Y.H., Hsu, P.H., Peng, S.H., Teng, Y.C., Kang, M.L., Wong, C.H., and Juan, L.J. (2014). O-GlcNAcylation regulates EZH2 protein stability and function. Proc. Natl. Acad. Sci. USA *111*, 1355–1360.

Das, F., Ghosh-Choudhury, N., Dey, N., Mandal, C.C., Mahimainathan, L., Kasinath, B.S., Abboud, H.E., and Choudhury, G.G. (2012). Unrestrained mammalian target of rapamycin complexes 1 and 2 increase expression of phosphatase and tensin homolog deleted on chromosome 10 to regulate phosphorylation of Akt kinase. J. Biol. Chem. *287*, 3808–3822.

Dentin, R., Hedrick, S., Xie, J., Yates, J., 3rd, and Montminy, M. (2008). Hepatic glucose sensing via the CREB coactivator CRTC2. Science *319*, 1402–1405.

Du, X.L., Edelstein, D., Dimmeler, S., Ju, Q., Sui, C., and Brownlee, M. (2001). Hyperglycemia inhibits endothelial nitric oxide synthase activity by posttranslational modification at the Akt site. J. Clin. Invest. *108*, 1341–1348.

Egan, D.F., Shackelford, D.B., Mihaylova, M.M., Gelino, S., Kohnz, R.A., Mair, W., Vasquez, D.S., Joshi, A., Gwinn, D.M., Taylor, R., et al. (2011). Phosphorylation of ULK1 (hATG1) by AMP-activated protein kinase connects energy sensing to mitophagy. Science *331*, 456–461.

Gao, W., Shen, Z., Shang, L., and Wang, X. (2011). Upregulation of human autophagy-initiation kinase ULK1 by tumor suppressor p53 contributes to DNA-damage-induced cell death. Cell Death Differ. *18*, 1598–1607.

Hanover, J.A., Krause, M.W., and Love, D.C. (2010). The hexosamine signaling pathway: O-GlcNAc cycling in feast or famine. Biochim. Biophys. Acta *1800*, 80–95.

Hara, T., Takamura, A., Kishi, C., Iemura, S., Natsume, T., Guan, J.L., and Mizushima, N. (2008). FIP200, a ULK-interacting protein, is required for autophagosome formation in mammalian cells. J. Cell Biol. *181*, 497–510.

Hosokawa, N., Hara, T., Kaizuka, T., Kishi, C., Takamura, A., Miura, Y., Iemura, S., Natsume, T., Takehana, K., Yamada, N., et al. (2009). Nutrient-dependent mTORC1 association with the ULK1-Atg13-FIP200 complex required for autophagy. Mol. Biol. Cell *20*, 1981–1991.

Hsu, P.P., Kang, S.A., Rameseder, J., Zhang, Y., Ottina, K.A., Lim, D., Peterson, T.R., Choi, Y., Gray, N.S., Yaffe, M.B., et al. (2011). The mTOR-regulated

phosphoproteome reveals a mechanism of mTORC1-mediated inhibition of growth factor signaling. Science *332*, 1317–1322.

Hwang, J.Y., Gertner, M., Pontarelli, F., Court-Vazquez, B., Bennett, M.V.L., Ofengeim, D., and Zukin, R.S. (2017). Global ischemia induces lysosomal-mediated degradation of mTOR and activation of autophagy in hippocampal neurons destined to die. Cell Death Differ. *24*, 317–329.

Itakura, E., and Mizushima, N. (2010). Characterization of autophagosome formation site by a hierarchical analysis of mammalian Atg proteins. Autophagy *6*, 764–776.

Itakura, E., Kishi, C., Inoue, K., and Mizushima, N. (2008). Beclin 1 forms two distinct phosphatidylinositol 3-kinase complexes with mammalian Atg14 and UVRAG. Mol. Biol. Cell *19*, 5360–5372.

Jang, H., Kim, T.W., Yoon, S., Choi, S.Y., Kang, T.W., Kim, S.Y., Kwon, Y.W., Cho, E.J., and Youn, H.D. (2012). O-GlcNAc regulates pluripotency and reprogramming by directly acting on core components of the pluripotency network. Cell Stem Cell *11*, 62–74.

Jung, C.H., Jun, C.B., Ro, S.H., Kim, Y.M., Otto, N.M., Cao, J., Kundu, M., and Kim, D.H. (2009). ULK-Atg13-FIP200 complexes mediate mTOR signaling to the autophagy machinery. Mol. Biol. Cell *20*, 1992–2003.

Kim, J., Kundu, M., Viollet, B., and Guan, K.L. (2011). AMPK and mTOR regulate autophagy through direct phosphorylation of Ulk1. Nat. Cell Biol. *13*, 132–141.

Kim, J., Kim, Y.C., Fang, C., Russell, R.C., Kim, J.H., Fan, W., Liu, R., Zhong, Q., and Guan, K.L. (2013). Differential regulation of distinct Vps34 complexes by AMPK in nutrient stress and autophagy. Cell *152*, 290–303.

Liang, C., Feng, P., Ku, B., Dotan, I., Canaani, D., Oh, B.H., and Jung, J.U. (2006). Autophagic and tumour suppressor activity of a novel Beclin1-binding protein UVRAG. Nat. Cell Biol. *8*, 688–699.

Matsunaga, K., Saitoh, T., Tabata, K., Omori, H., Satoh, T., Kurotori, N., Maejima, I., Shirahama-Noda, K., Ichimura, T., Isobe, T., et al. (2009). Two Beclin 1-binding proteins, Atg14L and Rubicon, reciprocally regulate autophagy at different stages. Nat. Cell Biol. *11*, 385–396.

Misra, S., Miller, G.J., and Hurley, J.H. (2001). Recognizing phosphatidylinositol 3-phosphate. Cell *107*, 559–562.

Mizushima, N., Yoshimori, T., and Levine, B. (2010). Methods in mammalian autophagy research. Cell *140*, 313–326.

Park, J.M., Jung, C.H., Seo, M., Otto, N.M., Grunwald, D., Kim, K.H., Moriarity, B., Kim, Y.M., Starker, C., Nho, R.S., et al. (2016). The ULK1 complex mediates MTORC1 signaling to the autophagy initiation machinery via binding and phosphorylating ATG14. Autophagy *12*, 547–564.

Pattingre, S., Bauvy, C., Carpentier, S., Levade, T., Levine, B., and Codogno, P. (2009). Role of JNK1-dependent Bcl-2 phosphorylation in ceramide-induced macroautophagy. J. Biol. Chem. *284*, 2719–2728.

Proikas-Cezanne, T., Takacs, Z., Donnes, P., and Kohlbacher, O. (2015). WIPI proteins: essential PtdIns3P effectors at the nascent autophagosome. J. Cell Sci. *128*, 207–217.

Ruan, H.B., Ma, Y., Torres, S., Zhang, B., Feriod, C., Heck, R.M., Qian, K., Fu, M., Li, X., Nathanson, M.H., et al. (2017). Calcium-dependent O-GlcNAc signaling drives liver autophagy in adaptation to starvation. Genes Dev. *31*, 1655–1665.

Schu, P.V., Takegawa, K., Fry, M.J., Stack, J.H., Waterfield, M.D., and Emr, S.D. (1993). Phosphatidylinositol 3-kinase encoded by yeast VPS34 gene essential for protein sorting. Science *260*, 88–91.

Shang, L., and Wang, X. (2011). AMPK and mTOR coordinate the regulation of Ulk1 and mammalian autophagy initiation. Autophagy *7*, 924–926.

Slawson, C., and Hart, G.W. (2011). O-GlcNAc signalling: implications for cancer cell biology. Nat. Rev. Cancer *11*, 678–684.

Sun, Q., Fan, W., Chen, K., Ding, X., Chen, S., and Zhong, Q. (2008). Identification of Barkor as a mammalian autophagy-specific factor for Beclin 1 and class III phosphatidylinositol 3-kinase. Proc. Natl. Acad. Sci. USA *105*, 19211–19216.

Takahashi, Y., Coppola, D., Matsushita, N., Cualing, H.D., Sun, M., Sato, Y., Liang, C., Jung, J.U., Cheng, J.Q., Mulé, J.J., et al. (2007). Bif-1 interacts with Beclin 1 through UVRAG and regulates autophagy and tumorigenesis. Nat. Cell Biol. *9*, 1142–1151.

Tarrant, M.K., Rho, H.S., Xie, Z., Jiang, Y.L., Gross, C., Culhane, J.C., Yan, G., Qian, J., Ichikawa, Y., Matsuoka, T., et al. (2012). Regulation of CK2 by phosphorylation and O-GlcNAcylation revealed by semisynthesis. Nat. Chem. Biol. *8*, 262–269.

Vocadlo, D.J. (2012). O-GlcNAc processing enzymes: catalytic mechanisms, substrate specificity, and enzyme regulation. Curr. Opin. Chem. Biol. *16*, 488–497.

Wang, Z., Gucek, M., and Hart, G.W. (2008). Cross-talk between GlcNAcylation and phosphorylation: site-specific phosphorylation dynamics in response to globally elevated O-GlcNAc. Proc. Natl. Acad. Sci. USA *105*, 13793–13798.

Wells, L., Kreppel, L.K., Comer, F.I., Wadzinski, B.E., and Hart, G.W. (2004). O-GlcNAc transferase is in a functional complex with protein phosphatase 1 catalytic subunits. J. Biol. Chem. *279*, 38466–38470.

Wong, P.M., Feng, Y., Wang, J., Shi, R., and Jiang, X. (2015). Regulation of autophagy by coordinated action of mTORC1 and protein phosphatase 2A. Nat. Commun. *6*, 8048.

Yang, W.H., Kim, J.E., Nam, H.W., Ju, J.W., Kim, H.S., Kim, Y.S., and Cho, J.W. (2006). Modification of p53 with O-linked N-acetylglucosamine regulates p53 activity and stability. Nat. Cell Biol. *8*, 1074–1083.

Yang, X., Ongusaha, P.P., Miles, P.D., Havstad, J.C., Zhang, F., So, W.V., Kudlow, J.E., Michell, R.H., Olefsky, J.M., Field, S.J., and Evans, R.M. (2008). Phosphoinositide signalling links O-GlcNAc transferase to insulin resistance. Nature *451*, 964–969.

Yi, W., Clark, P.M., Mason, D.E., Keenan, M.C., Hill, C., Goddard, W.A., 3rd, Peters, E.C., Driggers, E.M., and Hsieh-Wilson, L.C. (2012). Phosphofructokinase 1 glycosylation regulates cell growth and metabolism. Science *337*, 975–980.

Zalckvar, E., Berissi, H., Mizrachy, L., Idelchuk, Y., Koren, I., Eisenstein, M., Sabanay, H., Pinkas-Kramarski, R., and Kimchi, A. (2009). DAP-kinase-mediated phosphorylation on the BH3 domain of beclin 1 promotes dissociation of beclin 1 from Bcl-XL and induction of autophagy. EMBO Rep. *10*, 285–292.

Zeidan, Q., and Hart, G.W. (2010). The intersections between O-GlcNAcylation and phosphorylation: implications for multiple signaling pathways. J. Cell Sci. *123*, 13–22.

Zhong, Y., Wang, Q.J., Li, X., Yan, Y., Backer, J.M., Chait, B.T., Heintz, N., and Yue, Z. (2009). Distinct regulation of autophagic activity by Atg14L and Rubicon associated with Beclin 1-phosphatidylinositol-3-kinase complex. Nat. Cell Biol. *11*, 468–476.

Zhu, G., Tao, T., Zhang, D., Liu, X., Qiu, H., Han, L., Xu, Z., Xiao, Y., Cheng, C., and Shen, A. (2016). O-GlcNAcylation of histone deacetylases 1 in hepatocellular carcinoma promotes cancer progression. Glycobiology *26*, 820–833.

STAR★METHODS

KEY RESOURCES TABLE

REAGENT or RESOURCE	SOURCE	IDENTIFIER
Antibodies		
Rabbit polyclonal anti-Beclin1	Novus Biologicals	Cat#NB110-87318; RRID: AB_1201249
Rabbit polyclonal anti-LC3B	Novus Biologicals	Cat#NB100-2220; RRID: AB_10003146
Rabbit polyclonal anti-ULK1	Sigma Aldrich	Cat#A7481; RRID: AB_1840703
Mouse monoclonal anti-Flag	Sigma Aldrich	Cat#F3165; RRID: AB_259529
Rabbit polyclonal anti-ATG13	Sigma Aldrich	Cat#SAB4200100; RRID: AB_10602787
Mouse monoclonal anti-Phosphoserine	Sigma Aldrich	Cat#P5747; RRID: AB_477376
Mouse monoclonal anti-β-actin	Sigma Aldrich	Cat#A1978; RRID: AB_476692
Mouse polyclonal anti-PP1 (E-9)	Santa Cruz Biotechnology	Cat#sc-7482; RRID: AB_628177
Rabbit polyclonal anti-mTOR	Santa Cruz Biotechnology	Cat#sc-1549-R; RRID: AB_831568
Rabbit polyclonal anti-ATG14L	Abcam	Cat#Ab173943; RRID: N/A
Rabbit polyclonal anti-ATG101	Abcam	Cat# Ab105387; RRID: AB_10860488
Mouse polyclonal anti-O-linked N-acetylglucosamine (RLII)	Abcam	Cat#Ab2739; RRID: AB_303264
Rabbit polyclonal anti-OGT	Abcam	Cat#Ab96718; RRID: AB_10680015
Rabbit polyclonal anti-p-S757 ULK1	Cell Signaling Technology	Cat#6888; RRID: N/A
Rabbit polyclonal anti-p-S555 ULK1	Cell Signaling Technology	Cat#5869; RRID: N/A
Rabbit polyclonal anti-p-T172 AMPK	Cell Signaling Technology	Cat#2531; RRID: N/A
Rabbit polyclonal anti-p-S2448 mTOR	Cell Signaling Technology	Cat#2971S; RRID: N/A
Mouse monoclonal anti-HA	Covance	Cat#MMS-101R; RRID: AB_291263
Rabbit polyclonal anti-PPP5C	Bethyl Laboratories	Cat#A300-909A; RRID: AB_2168771
Bacterial and Virus Strains		
DH5-α *Escherichia coli*	Enzynomics	CP010
M15 pREP4 *Escherichia coli*	QIAGEN	32149
Chemicals, Peptides, and Recombinant Proteins		
Ni-NTA Agarose	QIAGEN	30210
cOmplete Protease Inhibitor Cocktail	Roche	11697498001
DMSO (vehicle)	Sigma Aldrich	D2650
Thiamet G	This paper	N/A
L-α-Phosphatidylinositol sodium salt	Sigma Aldrich	P0639
Torin 1	Tocris	4247
Tautomycetin	Tocris	2305
Compound C	Calbiochem	171260
N-Acetyl-D-glucosamine	Sigma Aldrich	A8625
ATP, [γ-^{32}P]	Perkin Elmer	NEG-002A
Silica gel HL, 250 micron (Thin Layer Chromatography)	Analtech	Z265519
Uridine 5′-diphospho-N-acetylglucosamine sodium salt	Sigma Aldrich	U4375
Deposited Data		
Raw data	Mendeley	https://data.mendeley.com/datasets/259594j572/1
Experimental Models: Cell Lines		
Human: H1299 cells	Dr. Chin Ha Chung Lab	N/A
Human: HEK293 cells	ATCC	CRL-11268
Human: SW620 cells	Dr. Chin Ha Chung Lab	N/A

(*Continued on next page*)

Continued

REAGENT or RESOURCE	SOURCE	IDENTIFIER
Oligonucleotides		
shRNA targeting sequence: PPP1CA: CCGGTGAGTGCAAGA GACGCTACAACTCGAGTTGTAGCGTCTCTTGCACTCATTTTT (Human Phosphatases Glycerol-1)	Sigma Aldrich	SH0411
shRNA targeting sequence: PPP5C: CCGGGAGACAGAGAAG ATTACAGTACTCGAGTACTGTAATCTTCTCTGTCTCTTTTT (Human Phosphatases Glycerol-1)	Sigma Aldrich	SH0411
siRNA targeting sequence: ULK1: GGAGAAAACTTGTAGGTGT	Gao et al., 2011	N/A
siRNA targeting sequence: OGT: GGAGGCTATTCGAATCAGT	This paper	N/A
Recombinant DNA		
Plasmid: pLKO.1-Puro	Sigma Aldrich	SH0111
Plasmid: CMV-Flag-ncOGT	Dr. Jin Won Cho Lab	N/A
Plasmid: 1xHA pcDNA-ncOGT	This paper	N/A
Plasmid: CMV10-3xFlag-ULK1 WT	This paper	N/A
Plasmid: CMV10-3xFlag-ULK1 Δ279-833	This paper	N/A
Plasmid: CMV10-3xFlag-ULK1 1-600	This paper	N/A
Plasmid: CMV10-3xFlag-ULK1 279-833	This paper	N/A
Plasmid: pcDNA-HA-ULK1 WT	This paper	N/A
Plasmid: pcDNA-HA-ULK1 T754N	This paper	N/A
Plasmid: pcDNA-HA-ULK1 T754Y	This paper	N/A
Plasmid: pcDNA-HA-ULK1 T754A	This paper	N/A
Plasmid: pcDNA-HA-ULK1 T754Q	This paper	N/A
Plasmid: pcDNA-HA-ULK1 S757A	This paper	N/A
Plasmid: pcDNA-HA-ULK1 T754N/S757A	This paper	N/A
Plasmid: pcDNA-HA-ULK1 S317A	This paper	N/A
Plasmid: pcDNA-HA-ULK1 S317D	This paper	N/A
Plasmid: pcDNA-HA-ULK1 S467A	This paper	N/A
Plasmid: pcDNA-HA-ULK1 S467D	This paper	N/A
Plasmid: pcDNA-HA-ULK1 S555A	This paper	N/A
Plasmid: pcDNA-HA-ULK1 S555D	This paper	N/A
Plasmid: pcDNA-HA-ULK1 T574A	This paper	N/A
Plasmid: pcDNA-HA-ULK1 T574D	This paper	N/A
Plasmid: pcDNA-HA-ULK1 S637A	This paper	N/A
Plasmid: pcDNA-HA-ULK1 S637D	This paper	N/A
Plasmid: pcDNA-HA-ULK1 S777A	This paper	N/A
Plasmid: pcDNA-HA-ULK1 S777D	This paper	N/A
Plasmid: pcDNA-HA-PPP1CA (PP1)	This paper	N/A
Plasmid: pcDNA-HA-PPP2A (PP2A)	Dr. Yong-Keun Jung Lab	N/A
Plasmid: pcDNA-HA-PPP5C (PP5)	Dr. Yong-Keun Jung Lab	N/A
Plasmid: EGFP-LC3	Dr. Chanhee Kang Lab	N/A
Plasmid: mCherry-GFP-LC3	Dr. Yong-Keun Jung Lab	N/A
Plasmid: Flag-mTOR-CA (I2017T, V2198A, L2216H, L2260P)	This paper	N/A
Software and Algorithms		
ImageJ 1.51k	Wayne Rasband, NIH	https://imagej.nih.gov/ij/download.html
Microsoft Excel 2016	Microsoft Office software	N/A
GraphPad Prism 5	GraphPad software	N/A

CONTACT FOR REAGENT AND RESOURCE SHARING

Further information and requests for reagents may be directed to and will be fulfilled by the Lead Contact, Sung Hee Baek (sbaek@snu.ac.kr).

EXPERIMENTAL MODEL AND SUBJECT DETAILS

Cell lines

HEK293 cells were cultured in DMEM supplemented with 5% fetal bovine serum and penicillin (40 U/ml)/streptomycin (40 mg/ml) at 37°C under 5% CO2. H1299 and SW620 cells were cultured in RPMI1640 supplemented with 5% fetal bovine serum and penicillin (40 U/ml)/streptomycin (40 mg/ml) at 37°C under 5% CO2. Cells were transfected using Lipofectamine 3000. For cells that were treated with glucose starvation, glucose free DMEM or RPMI1640 supplemented with 5% dialyzed fetal bovine serum was used.

METHOD DETAILS

Cell culture

HEK293, H1299, and SW620 cell lines were cultured in DMEM (Welgene, South Korea, LM001-05) or RPMI1640 (Welgene, South Korea, LM011-01) supplemented with 10% (v/v) fetal bovine serum (GIBCO, 26140-079), 100 U/ml penicillin and 100 μg/ml streptomycin (Welgene, South Korea, LS-20301). All cell lines used were regularly tested for mycoplasma contamination. Lipofectamine 3000 (Life Technologies, 100022052) and Gene In (Global Stem, catalog# 73802, 73012) transfection reagents were used and transfection was performed according to the manufacturers' protocol. Cells were harvested 24 to 36 h post-transfection. Experiments were performed under normal growth conditions, unless otherwise stated. For starvation, cells were washed twice in phosphate-buffered saline (Welgene, South Korea, LB001-02) and incubated in glucose-free DMEM (Welgene, South Korea, LM001-56) or RPMI1640 (Welgene, South Korea, LM011-60) supplemented with dialyzed fetal bovine serum (TCB, 101DI) for indicated hours.

Generation of ULK1$^{-/-}$ cells using CRISPR/Cas9

To generate KO cells, cells were transfected with px330 plasmids having following sequence: *ULK1* Fw-5′-AGCAGATCGCGGGCGC CATG-3′, Rv-5′-CATGGCGCCCGCGATCTGCT-3′. After transfection, single cells were grown until colonies form. KO cells were selected based on protein expression and genomic DNA sequencing.

LC-ETD-MS/MS analysis

Flag-tagged ULK1 was coexpressed with OGT to induce O-GlcNAcylation. ULK1 was immunopurified using M2 beads, washed and eluted. The protein was denatured with 8 M urea in 50 mM ammonium bicarbonate (ABC) and followed by reduction and alkylation of cysteine thiols. After dilution to 1 M urea concentration with 50 mM ABC buffer, protein digestion by trypsin was performed at 37°C for overnight. SPE clean up and sample concentration in speed-vac was preceded before mass spec analysis. LC-ETD-MS/MS experiment was performed on Orbitrap Fusion Lumos mass spectrometry (Thermo Fisher Scientific) coupled with nanoACQUITY UPLC (Waters) equipped with an in-house packed capillary analytical column (75 μm x 100 cm) and trap column (150 μm x 3 cm) with 3 μm Jupiter C18 particles (Phenomenex). The acquired ETD-MS/MS dataset was searched by MS-GF+ algorithm at 10 ppm of precursor ion mass tolerance against the SwissProt *Homo sapiens* proteome database.

Plasmids

Px330 sgRNA cloning vector for generating CRISPR Cas9 KO for *ULK1* was acquired from Addgene (#42230). Sequence for siULK1 has been described previously (Gao et al., 2011). Mutations were introduced using *n*Pfu-Forte mutagenesis kit (Enzynomics, P410).

Antibodies and reagents

Anti-Beclin1 antibody (NB110-87318) and anti-LC3B antibody (NB100-2220) were purchased from Novus Biologicals. Anti-ULK1 antibody (A7481), anti-Flag antibody (F3165), anti-ATG13 antibody (SAB4200100), anti-p-serine antibody (P5747), anti-β-actin antibody (A1978) were from Sigma Aldrich; anti-PP1 antibody (sc-7482), anti-mTOR antibody (sc-1549-R) were from Santa Cruz Biotechnology; anti-ATG14L antibody (Ab173943), anti-ATG101 antibody (Ab105387), anti-O-linked N-acetylglucosamine RLII antibody (Ab2739), and anti-OGT antibody (Ab96718) were from Abcam; anti-p-S757 ULK1 antibody (#6888), anti-p-S555 ULK1 antibody (#5869), anti-p-T172 AMPK antibody (#2531), anti-p-S2448 mTOR antibody (#2971S) and anti-VPS34 antibody (#3811S) were from Cell Signaling; anti-HA antibody (#MMS-101R) was from Covance; anti-PP5 antibody (A300-909A) was from Bethyl Laboratories; L-α-Phosphatidylinositol sodium salt (P0639) was from Sigma Aldrich; WGA beads (AL-1023S) were from Vector Laboratories; Torin 1 (4247) and tautomycetin (2305) were from Tocris. Transfection was performed with Lipofectamine 3000 (Invitrogen) according to the manufacturer's protocol.

Co-immunoprecipitation assays

All cells were briefly rinsed with ice-cold PBS before collection. Cells were lysed in EBC200 buffer (50 mM Tris-HCl [pH 8.0], 0.2 M NaCl, 0.5% NP-40, and protease inhibitors) on ice for 30 min. The lysates were collected and cleared by centrifugation at 14,000 × g

for 10 min at 4°C. Total protein concentration in the lysates was determined using the Bio-Rad Protein Assay Dye Reagent Concentrate (Bio-Rad, #500-0006). For co-immunoprecipitation assays, lysates were immunoprecipitated with protein A- and protein G-Sepharose beads (GE Healthcare) for 2-4 hours with indicated antibodies. The beads were pelleted and washed five times in EBC200 buffer and then resuspended in SDS-PAGE-loading buffer. Bound proteins were eluted by boiling, resolved by SDS-PAGE, followed by immunoblot analysis. The blots were blocked and incubated in PBS containing 3% BSA and indicated antibody for 2-4 hours. After six 10-min washes in 0.1% Triton X-100 in PBS (PBS-T), the blots were incubated in horse radish peroxidase-conjugated secondary antibody in PBS-T/ 3% BSA for 1-2 hours. For detection of bound proteins, the blots were washed five times in PBS-T, and then incubated in ECL.

Immunofluorescence microscopy

Cells grown on coverslips at a density of 7×10^4 cells were washed three times with PBS and then fixed with 2% paraformaldehyde in PBS for 10 min at room temperature. Fixed cells were permeabilized with PBS-T for 10 min at room temperature. Blocking was performed with 3% bovine serum in PBS-T for 30 min. For staining, cells were incubated with indicated antibodies for 4 hours at room temperature, followed by incubation with fluorescent labeled secondary antibodies for 1 hour. The following fluorescent secondary antibodies were used: donkey anti-mouse IgG; AlexaFluor 488, AlexaFluor 594; donkey anti-rabbit IgG AlexaFluor 488, AlexaFluor 594 (all from Invitrogen). Cells were mounted and visualized under a confocal microscope (Zeiss, LSM700). For autophagy studies, cells were transfected with GFP-LC3/mCherry-GFP-LC3 and sub-cultured onto coverslips followed by glucose starvation and fixation. For co-localization studies, cells were transfected with HA-PP1/Flag-ULK1 and sub-cultured onto coverslips followed by glucose starvation and fixation. The following day, cells were incubated with either complete media or glucose starvation media for indicated times.

In vitro kinase assay

ULK1 proteins were immunoprecipitated from HEK293 cell with anti-Flag M2 agarose affinity gel (Sigma). The immune-complex was extensively washed with BC150 (20 mM Tris-HCL, pH 7.9, 15% glycerol, 1 mM EDTA, 1mM DTT (dithiothreitol), 0.05% NP40, and 150 mM KCl for three times, and with BC300 (same as BC150 except for 300 mM KCl) for three times, and lastly with BC150 for three times. Flag-peptide was used for elution from the affinity gel. His-ATG14L proteins were purified from *E. coli* strain M15pRep using Ni-NTA resin (QIAGEN). ULK1 and ATG14L proteins were incubated in kinase assay buffer containing 10 mM HEPES at pH 7.4, 50 mM NaCl, 10 mM $MgCl_2$, 10 mM $MnCl_2$, 1 mM DTT, protease inhibitors. 10 μM cold ATG and 10 μCi [γ-^{32}P]ATP were added per reaction. The kinase reaction was performed at 37°C for 30 min and the reaction was terminated by adding SDS sample buffer and subjected to SDS–PAGE (polyacrylamide gel electrophoresis) and autoradiography.

In vitro VPS34 lipid kinase assay

Flag-tagged VPS34-expressing HEK293 cells were immunoprecipitated with anti-Flag M2-agarose affinity gel as immunoprecipitation assay and washed with NP-40 buffer, eluted with 3X Flag peptide in TBS buffer (150 mM NaCl, 50 mM Tris-HCl [pH 7.4]). Immuno-purified complexes were equilibrated in kinase base buffer (20 mM HEPES [pH 7.4], 1 mM EGTA, 0.4 mM EDTA, and 5 mM $MgCl_2$) and then preincubated for 10 min at room temperature with 10 mM $MnCl_2$ and 2 μg sonicated phosphatidylinositol (Sigma). 10 μCi [γ-^{32}P] ATP and 1 mM cold ATP were added and incubated for 15 min at room temperature. The kinase reactions were stopped by directly adding 10 μL 1 M HCl, followed by lipid extraction with 2 volumes of methanol/$CHCl_3$ (1: 1). Samples were vortexed and centrifuged at maximum speed for 10 min. The organic phase was loaded on a thin-layer chromatography plate (Analtech). Resolution of phospho-lipid was achieved using a buffer composition of $CHCl_3$/methanol/NH_4OH (30%)/ water (129: 100: 4.29: 24). Resolved plates were analyzed by autoradiography.

In vitro OGT assay

Recombinant Flag-OGT protein purified from HEK293 cells and recombinant 6X His-tagged ULK1 protein purified from *E. coli* were mixed in the reaction buffer (50 mM Tris-HCl pH 7.5, 12.5 mM $MgCl_2$, 2 mM UDP-GlcNAc, 1 mM DTT) in a final volume of 25 μl per sample. The samples were incubated at 37°C for 24 hours. The reaction was resolved with SDS-PAGE, blotted onto a polyvinylidene difluoride (PVDF) membrane, followed by immunoblotting with anti-O-GlcNAc antibody to detect O-GlcNAcylation of ULK1.

QUANTIFICATION AND STATISTICAL ANALYSIS

All experiments were performed independently at least three times. Values are expressed as mean ± s.e.m. Significance was analyzed by one-tailed, unpaired t test or one-way ANOVA using GraphPad Prism software. $p < 0.05$ was considered statistically significant. *$p < 0.01$, **$p < 0.001$, ***$p < 0.0001$.

DATA AND SOFTWARE AVAILABILITY

Raw data have been deposited to Mendeley Data and are available at https://data.mendeley.com/datasets/259594j572/1.